Sensing and Bio-Sensing Research 21 (2018) 54–64

Contents lists available at ScienceDirect

Sensing and Bio-Sensing Research

journal homepage: www.elsevier.com/locate/sbsr

Lactate Dehydrogenase and Glutamate Pyruvate Transaminase biosensing strategies for lactate detection on screen-printed sensors. Catalysis efficiency and interference analysis in complex matrices: from cell cultures to sport medicine

Giulio Rosati[a,*], Gaia Gherardi[b], Davide Grigoletto[b], Giuseppe Marcolin[b], Pasqua Cancellara[b], Cristina Mammucari[b], Matteo Scaramuzza[c], Alessandro De Toni[c], Carlo Reggiani[b], Rosario Rizzuto[b], Alessandro Paccagnella[a]

[a] Department of Information Engineering, via G. Gradenigo, 6b, University of Padova, 35131 Padova, Italy
[b] Department of Biomedical Sciences, University of Padova, via U. Bassi, 58, 35131 Padova, Italy
[c] ARC – Centro Ricerche Applicate s.r.l., via J. Da Montagnana, 49, 35132 Padova, Italy

ARTICLE INFO

Keywords:
Lactic acid
SPCE
Cyclic voltammetry
Sweat
Cell cultures
DMEM

ABSTRACT

Lactate detection with electrochemical biosensors is a fundamental part of the sensing and biosensing research field. Together with glucose detection, this topic attracted scientist attention since the 60s. Lactate is a metabolite involved in many processes among several fields of application, from food degradation, to sport medicine, cell cultures analysis, and clinical monitoring. However, few electrochemical lactate biosensors are currently present in the market.

In this work, we analyzed and compared the standard Lactate Dehydrogenase catalysis mechanism with a two-enzymes commercial method that proved to dramatically boost the catalysis efficiency from 0.6% to 72.5%. Both the mechanisms result in the production of reduced Nicotinamide Adenine Dinucleotide (NADH). Therefore, we analyzed its electrochemical detection performance using commercial screen-printed carbon electrodes (SPCE), along with the possible interferences of common mediums and buffers. We found that these sensors can be used for NADH detection down to a 10 μM concentration with a sensitivity of 33.14 nA/μM at a 456 mV overpotential. Moreover, we analytically defined the interferences effects of Dulbecco's Modified Eagle Medium on the sensors by Electrochemical Impedance Spectroscopy measurements and equivalent electrical circuits modeling.

Finally, we tested the two-enzyme method in two case studies, i.e., cell cultures lactate monitoring as a valuable tool to evaluate their growth, and lactate quantification in human sweat to monitor physical exercise intensity. We proved the feasibility of the combination of commercial two-enzymes kit and SPCE as a low-cost, accurate, and sensitive lactate biosensor in different applications, regardless of sample interferences.

1. Introduction

Lactate (LA) detection is an evergreen research theme since its applications spans over an extremely wide range of sectors. Many different approaches have been developed for its detection since the 60s. However, few biosensors examples can be found in the market offer. Lactate biosensors are usually based on enzymes that catalyze a lactate reaction oxidizing or reducing an electroactive component present in the testing solution. The first generation of these biosensors reduced dissolved oxygen in hydrogen peroxide in presence of lactate and oxidized it back to oxygen at the electrode, quantifying the related current. The second generation of lactate biosensors adopted artificial redox

Abbreviations: AC, Alternate Current; CV, Cyclic Voltammetry; DC, Direct Current; DMEM, Dulbecco's Modified Eagle Medium; DSC, DropSens Carbon; EIS, Electrochemical Impedance Spectroscopy; FBS, Fetal Bovine Serum; GPT, Glutamate-Pyruvate Transaminase; HBRS, HEPES-Buffered Ringer's Solution; LA, Lactic Acid; LDH, Lactate Dehydrogenase; LOD, Limit Of Detection; NAD, Nicotinamide Adenine Dinucleotide; NADH, reduced Nicotinamide Adenine Dinucleotide; PA, Pyruvic Acid; PBS, Phosphate Buffered Saline; PPO, Peak Power Output; SPCE, Screen Printed Carbon Electrode; SR, Sweat Rate

* Corresponding author.
E-mail address: giulio.rosati.1@unipd.it (G. Rosati).

https://doi.org/10.1016/j.sbsr.2018.10.004
Received 28 June 2018; Received in revised form 12 October 2018; Accepted 17 October 2018

mediators such as ferrocyanide, added to the sample solution to better control and optimize the charge transfer. It is also possible to use "natural" redox mediators by choosing particular enzymes whose co-factor can be oxidized or reduced at appropriate potentials, i.e. Lactate Dehydrogenase (LDH) with Nicotinamide Adenine Dinucleotide (NAD). Finally, the third generation of lactate biosensors relies on the electrode surface nanofabrication to promote direct and mediator-free charge transfer between the enzyme oxidizing lactate and the electrode [1]. Less common technologies that allow lactate detection are molecularly imprinted polymers (MIP) and aptamers. In these cases, the specific recognition of lactate is performed by an affinity strategy. In the MIP case, the electrode surface is covered by a polymeric material shaped to specifically host the lactate molecule, if present in the sample [2]. However, the interferences in this kind of detection method are often not negligible. In the aptamers case, the electrode surface is functionalized with ssDNA strands with a particular folding able to specifically bind the lactate molecule but research is still going on developing stable and sensitive aptamers for such small molecules. For these reasons, the enzymatic methods are still driving the academic and market scenarios.

Within the enzyme-based method, metabolites like lactate and glucose are usually quantified by two enzyme families: oxidase enzymes, which catalyze the lactate conversion in pyruvate with the production of hydrogen peroxide [3,4], and dehydrogenase enzymes, catalyzing the metabolites dehydrogenation and, at the same time, the NAD^+ cofactor reduction to NADH (Scheme 1a). Therefore, the NADH detection plays an important role for the electrochemical determination of these metabolites [5–10]. Indeed, great attention has been directed in recent years towards the development of electrodes for the NADH amperometric detection at low voltages, reducing the interferences from other compounds and improving the detection limit and sensitivity [11]. So far, this goal has been pursued by two main strategies, i.e., studying new mediators for the NADH electrocatalysis [12–17], and investigating new materials for the direct NADH oxidation overpotential reduction [18–23]. Screen-printed carbon electrodes (SPCE) are a good compromise between manufacturing costs and NADH detection voltage [20,24–26]. However, low or no attention at all was directed to the investigation of the interference effects that cell culture mediums may have on these electrodes [21,27,28]. Since NADH could be easily detected on these sensors, another relevant problem that is usually ignored is the low efficiency of the most common Lactate Dehydrogenase isoform, i.e., the rabbit muscle one, which favors the PA to LA reaction instead of the LA catalysis [29]. This issue has been addressed in many ways during the years, but there is no evidence in literature of an easy and practical solution that enables a low-cost biosensor-based high efficiency LA detection.

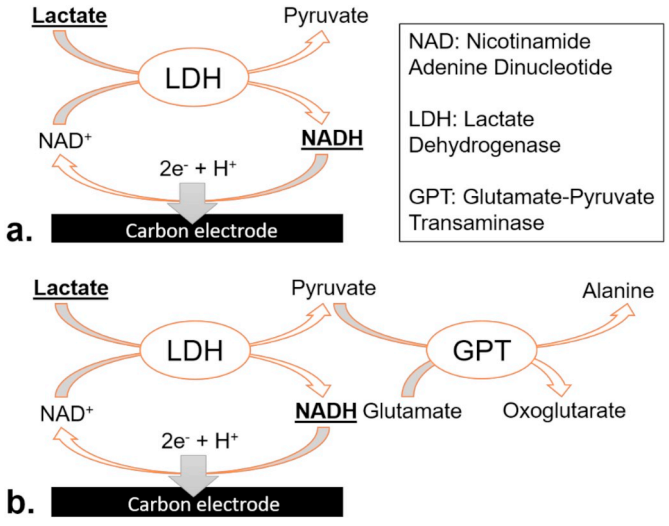

Scheme 1. Lactate electrochemical detection mechanisms based on LDH (a), and on the combined action of LDH and GPT (b). In both the cases, NADH produced by the lactate catalysis is oxidized at the electrode surface but in (b) the efficiency of the catalysis is boosted by the pyruvate depletion by GPT.

Monitoring metabolites' concentrations such as glucose and lactate in cell cultures gives useful insights on the cells' state and on the cell cultures development level [30,31]. The detection could be performed both by optical and electrochemical sensors [32–34] based on the described detection methods. However, their continuous and real-time electrochemical monitoring is rarely performed in the practice because of possible interferences by other compounds and by the cell mediums components [27,35]. To bypass these problems, the cells' state is often monitored through electrochemical impedance spectroscopy (EIS) measurements [36–39]. However, the impedance readout usually does not take care of suspended cells but just of those adhered onto the electrodes surface, and often requires the use of expansive microelectrodes arrays. To address the cost problem, all polymer electrodes and micro-devices were developed so far [40,41]. However, they cannot give the same specific information of the cells' metabolites detection.

Lactate is also correlated to hypoxia in the muscles during anaerobic physical exercise. Therefore, its monitoring is a precious parameter to define the sport training type and the respective performances [42,43]. Although blood or plasma analysis are the most characterized samples for this application, less invasive sensors (e.g. wearable sensors for sweat analysis) are requested by the market [44–46].

In this work, we studied and compared two LDH enzyme-based strategies for lactic acid detection with electrochemical biosensors. First, we used LDH alone, defining the catalysis kinetics and a measurement protocol to minimize the interferences of other compounds in the samples. In particular, we focused on cell cultures mediums, e.g., Dulbecco's Modified Eagle Medium (DMEM). Then, we studied the combination of the LDH enzyme with a second enzyme, i.e., Glutamate Pyruvate Transaminase (GPT), to improve the catalysis efficiency and to reduce the biosensor reactivity to interferences.

To compare the lactate detection performances with the LDH and LDH-GPT protocols on SPCE, we started from the study of the NADH electrochemical detection. We compared Cyclic Voltammetry (CV) and Amperometry, and we defined a NADH calibration curve, validated by standard UV–Visible spectroscopy measurements. We studied the interferences of culture mediums and buffers on the NADH detection by several ad-hoc protocols and also by EIS measurements and equivalent electrical modeling. Therefore, we obtained the NADH detection sensitivity, Limit of detection (LOD), and reproducibility in the mediums/buffers on SPCEs. Then, we studied the LDH kinetics by the standard Michaelis-Menten model and we verified the correlation of the CV and UV–Vis LA measurements. After that, we compared the catalysis efficiency of the LDH and LDH-GPT protocols in terms of the obtained NADH concentration with respect to the lactate one.

To demonstrate the ease of use and the efficiency of the LDH-GPT protocol, we tested it with two sample types, i.e., cell cultures in standard mediums such as DMEM, and human sweat samples collected during physical exercise at controlled intensity.

The tested samples contain a wide range of possible interfering compounds. Therefore, the lack of interference with the developed protocol will prove its suitability for most of the lactate detection applications.

2. Materials and methods

2.1. Reagents and SPCEs

All the reagents used in this work were purchased from Sigma-Aldrich (Merck), if not differently specified. The NAD oxidized (cod. N7004) and reduced (cod. N8129) forms were purchased as powders with a purity degree > 96.5%. All the NAD and NADH solutions were prepared in Tris-HCl buffer, pH of 8.8, and kept in the dark to avoid degradation. L-Lactic acid (cod. L1750) and pyruvic acid (cod. 107,360)

were purchased with a purity level > 98%, in powder and liquid forms, respectively. A 1 mM dilution of ferro/ferricyanide in 10 mM phosphate buffered saline (PBS) was used as redox mediator for the EIS measurements. PBS was prepared dissolving pre-weighted pouches in milliQ ultrapure water (18.2 MΩ cm). Tris-HCl was prepared by using Trizma® base with a 50 mM concentration and adding 1 M HCl to a pH of 8.8.

Dulbecco's Modified Eagle Medium (DMEM) was used as purchased. Hepes-Buffered Ringer's Solution (HBRS) was prepared ad-hoc (composition reported in Table A.1).

LDH isolated from rabbit muscle was bought dehydrated in 5 kU per pack (cod. L1254). The enzymes were suspended at a concentration of 100 U/ml in 10 mM PBS and divided in 10 µl aliquots, then stored at −20 °C.

The lactate detection tests with the LDH-GPT protocol were performed using the L-Lactic Acid Assay Kit™ by Megazyme and mixing its components as reported in Table A.2.

The electrochemical sensors used for the NADH electrochemical detection were purchased from DropSens (C-110, called DSCs in the following). They are composed by 3 screen-printed electrodes on a ceramic substrate. Working and counter electrodes are made of carbon, while the reference electrode is made with a silver ink. A solution volume of 100 µl was used for each test. The DSCs were thoroughly rinsed in milliQ water before any measurement.

2.2. NADH detection

The lactate detection by LDH catalysis is based on the NADH quantification. Since molecule can be detected both electrochemically and optically, we used UV–Visible spectrometry as control technique for NADH quantification by measuring the solutions absorbance at 340 nm. At this wavelength, NADH absorbs with a millimolar extinction coefficient of 6.3 Abs $mM^{-1}\,cm^{-1}$. Conversely, NAD absorbs only at 260 nm, thus the two forms can be easily distinguished and quantified. For the UV–Vis measurements we used a Mapada UV1600-PC spectrophotometer and quartz cuvettes with a pathlength of 1 cm.

The electrochemical NADH detection and quantification was performed both by cyclic voltammetry (CV) and amperometry, with a CH440a potentiostat connected to the DSCs through a DropSens adapter. We measured NADH dilutions ranging from 1 µM to 10 mM, logarithmically distributed with one point per decade of concentration. We performed the CVs varying the tension between 0 and 800 mV, with a 100 mV/s scan rate and a sensitivity of 10 µA/V. Regarding the amperometries, we performed measurements in 1 mM NADH in Tris-HCl testing different potentials from −400 mV to 800 mV, to define the lowest potential that shows the highest current response related to the NADH oxidation.

We performed the NADH calibration in Tris-HCl with both CVs and amperometries. Then, we compared the obtained calibration curves to select the technique with the widest linear range and the highest sensitivity.

2.3. Interference characterization

Once defined the best electrochemical technique, we studied the possible interference effects of common cell cultures mediums and buffers, such as DMEM, HBRS, and PBS. We performed EIS measurements in 1 mM ferro/ferricyanide in PBS, then 75 CV cycles in the mediums or buffer, and finally another set of EIS measurements. The comparison between the EIS spectra before and after the CVs allow to define the mediums/buffers effect on the DSCs surface. The EIS measurements were performed on 3 DSCs per each medium/buffer, in the 1 Hz- 100 kHz frequency range with an applied AC tension of 5 mV and a DC bias equal to the ferro/ferricyanide standard reduction potential (E^0) on DSCs, i.e., 110 mV. We analyzed the EIS data by equivalent electrical circuit (EEC) modeling with the circuits shown in Scheme 2.

We used two different EECs because the CVs in DMEM caused variations that made the conventional Randles cell model shown in Scheme 2a inadequate to fit those EIS spectra.

To assess the effect of the mediums/buffer on the NADH detection, we performed a CV calibration in each medium/buffer with NADH concentrations ranging from 1 µM to 1 mM, with 3 dilutions per decade. The calibration was performed both repeating the measurements on the same DSCs (from the lowest to the highest concentration) and in changing the DSC for each NADH concentration. In the following, we will refer to the first as repeated measurements, and to the second as one-shot measurements. The comparison between the repeated and one-shot measurements allow to assess the possibility to use the device more than once, for each medium/buffer.

2.4. Lactic acid catalysis study

We studied the lactate catalysis, with the configuration showed in Scheme 1a, mixing NAD, LDH, and LA. Ten LA dilutions in HBRS and three LDH concentrations were considered, while the NAD concentration was 500 µM in all the tests. We monitored the NADH formation at 340 nm by UV–Vis kinetic measurements. The data collected in this study was fitted by the standard Michaelis-Menten kinetic model, defining the LDH concentration to obtain fast and effective LA catalysis.

To prove the correlation between the NADH concentrations measured by the two techniques, the same experiment was repeated with the defined LDH concentration, and measuring the produced NADH also by CVs, testing 100 µl of the cuvette solution on 3 DSCs after the 5 min UV–Vis measurements.

The same LA dilutions tested before were used also with the LDH-GPT protocol (Scheme 1b), detailed in Table A.2. Again, both UV–Vis and CV measurements were performed. The comparison of the LDH and LDH-GPT protocols was performed by means of the respective catalysis efficiencies, defined as the percentage ratio of the produced NADH and the tested LA concentrations, and the traditional performance factors, i.e., LOD, sensitivity, linear range, and response time.

2.5. Case 1: cell cultures analysis

The cell culture samples were collected from HeLa cells cultured for 72 h in DMEM, at times of 0, 24, 48, and 72 h. Pure medium samples, maintained in identical conditions, were collected at the same times to be used as negative control. The tests were carried out cultivating the cells in 6 wells plates both with and without Fetal Bovine Serum (FBS), to test its possible interference effects on the detection. In fact, FBS contains a low concentration of lactate itself and, since its composition is quite variable, the FBS exclusion from the measurements shall result in a higher reproducibility. However, the negative control samples shall

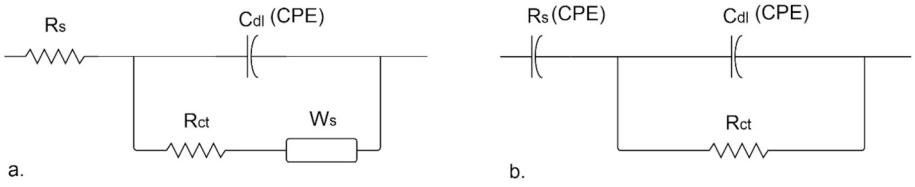

Scheme 2. Equivalent electrical circuits used to model the EIS data before and after the HBRS and PBS CVs (a) and after the DMEM CVs (b).

allow to perform differential measurements, depleting the FBS interferences. After each sampling, the cells were counted by means of Scepter 2.0 Cell Counter (Millipore) to monitor their actual growth both in DMEM and in DMEM + FBS.

2.6. Case 2: sweat analysis

The sweat samples were collected from healthy volunteers during two physical exercise tests in a controlled environment (25°, 60% R.H.). During the first test, 4 volunteers were asked to perform a 60 min exercise with a constant cadence on a cycle ergometer. The power output was imposed as the 45% of their previously measured peak power output (PPO). The sweat samples were collected from the forearm every 10 min by capillaries and sterilized gauzes. During sampling, the cardiac frequency and respiratory quotient were measured and the perceived effort quantify by means of a Borg CR-10 scale [47].

For the second test, a single volunteer performed a 40 min' increasing intensity exercise with a peak of 86% of his PPO. Three sweat samples were collected by sterilized gauzes attached on the volunteer back and sealed with 14 × 14 cm waterproof bandage. For each sample, a different gauze was removed from the volunteer back, weighted, and centrifuged to obtain the liquid sample. Thanks to the gauze weighting, we could define the sweat rate (SR) as shown in eq. 1:

$$SR = \frac{m_{sweat}}{Area \bullet Time} \quad (1)$$

During both the experiments, capillary blood lactate was measured by a Lactate Scout™ (SensLab GmbH) from the volunteer ear, in parallel with sweat sampling. All the samples were stored at −80 °C until tests were performed.

3. Results and discussion

3.1. NADH detection

The NADH electrochemical detection and quantification was performed by Cyclic Voltammetry (CV) and amperometry on DSC sensors. We prepared a 1 mM NADH dilution in 50 mM Tris-HCl and we performed amperometries with different DC voltages from 0 to 800 mV. The same solution was then tested on DSC sensors by CV at 100 mV/s in the same voltage range. We obtained the current curves reported and compared in Fig. 1a.

The NADH oxidation produces negative currents within the potentiostat reference system (anodic positive). The curves in fig. 1a show appreciable kinetics only for voltages over 400 mV, with current values saturating in < 5 s. Coherently with the CV, both the starting and final current values decrease between 200 mV and 500 mV. The current variations are less relevant for voltages over 600 mV, thus we chose 600 mV as DC tension for the following amperometries. The CV curve showed an oxidation peak at 525 mV and took 12 s to be performed.

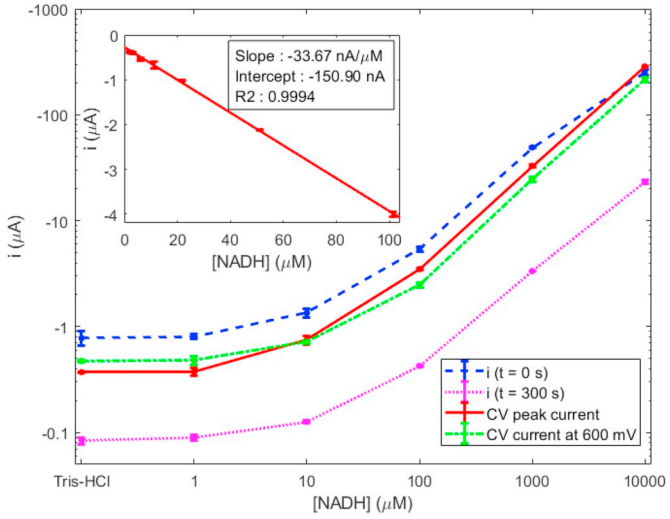

Fig. 2. Calibration curves obtained by the i-t curves initial and final currents (600 mV), and by the CV peak currents and the 600 mV current values. The NADH calibration by the CV peak current values is represented in the inset.

In order to choose between the techniques for NADH detection, we prepared NADH dilutions between 1 μM and 10 mM, we verified them by UV–Vis measurements at 340 nm, and we performed both amperometry and CVs on different DSCs. In Fig. 1b we show the results of this measurements for the lowest NADH concentrations, i.e., 1, 10, 100 μM. In Fig. 5, we report the NADH calibration curves obtained by the 0 s and 300 s current values of the amperometries, and the peak and 600 mV currents recorded by the anodic sweep of the CVs.

We selected CV as NADH detection technique and its peak current values as quantification parameter since it showed the highest variations in the NADH tested range, as depicted in Fig. 2. The NADH calibration with this parameter shows a linear response in the 0–100 μM range (Fig. 2 inset), with a sensitivity of 36.67 nA/μM.

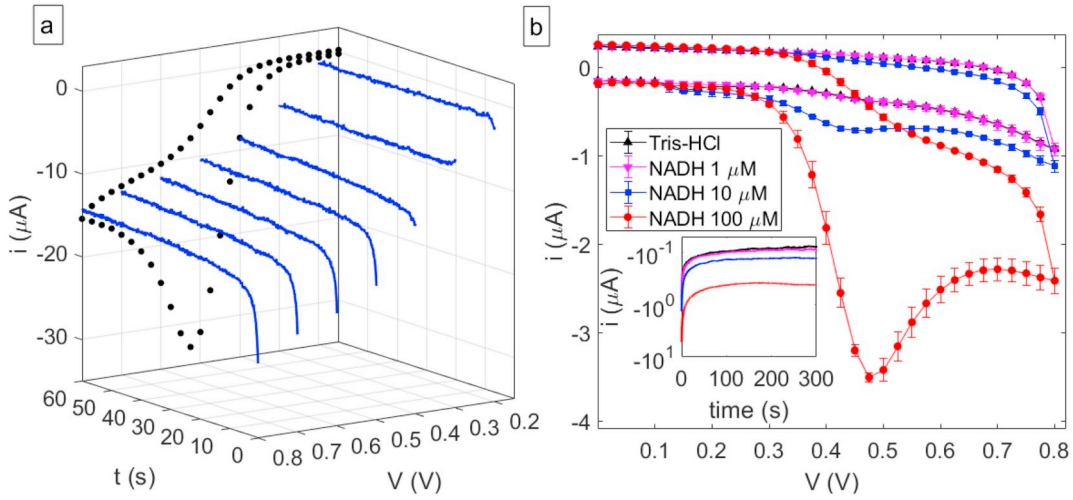

Fig. 1. (a) amperometries obtained by constant voltages between 200 mV and 800 mV on DSCs in 100 μl of 1 mM NADH in 50 mM Tris-HCl and Cyclic Voltammetry obtained on DSCs in the same solution at 100 mV/s (projected to the 60 s plane). (b) CV curves and amperometries (inset) obtained with NADH concentrations from 0 to 100 μM.

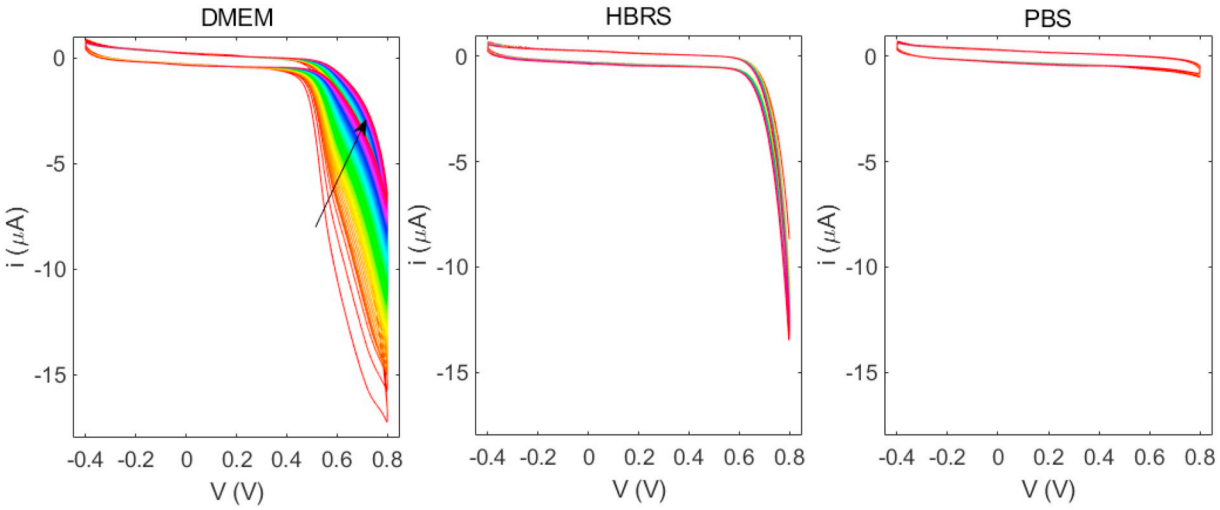

Fig. 3. CVs obtained from the 75 cycles in DMEM, HBRS, and PBS medium/buffers. The cycling order is described by colors from red to purple, as indicated by the arrow. (For interpretation of the references to colour in this figure legend, the reader is referred to the web version of this article.)

3.2. Interference characterization

To define cell mediums/buffers effects on the DSC sensors, we performed an impedimetric study in 1 mM ferro/ferricyanide. We measured EIS sweeps on 9 DSC sensors with a DC voltage of 110 mV. Then, we measured 75 CV cycles in DMEM, HBRS, and PBS on 3 DSCs per each medium/buffer. Finally, we tested again all the sensors by EIS sweeps with the same protocol of the former measurements. The CV results of one DSC per each tested medium/buffer are showed in Fig. 3, while the Bode diagrams of the average impedance spectra are depicted in Fig. 4.

The CV data show oxidation currents by both DMEM and HBRS at potentials over 500 mV and 600 mV, respectively. However, HBRS presents slight variations among the various CV cycles. PBS does not show any significant current peak but just the hysteresis curve due to the double layer capacitance of the electrode's interface.

The Bode diagrams show that the PBS and HBRS curves are close to the pre-CV measurements, with slight difference in correspondence to the capacitive phase peak at 100 Hz. Generally, these curves show a resistive part related to the solution resistance R_s and a capacitive part due to the double layer capacitance C_{dl}, in the 100 KHz and 100 Hz regions, respectively. At lower frequencies, we can see a charge transfer contribution around 1 Hz (modeled by R_{ct}), and a typical Warburg diffusion response at lower frequencies. Therefore, the pre-CV, HBRS, and PBS spectra are modeled by Randles cell (Scheme 1a) with excellent fit quality (χ^2 values lower than 0.001).

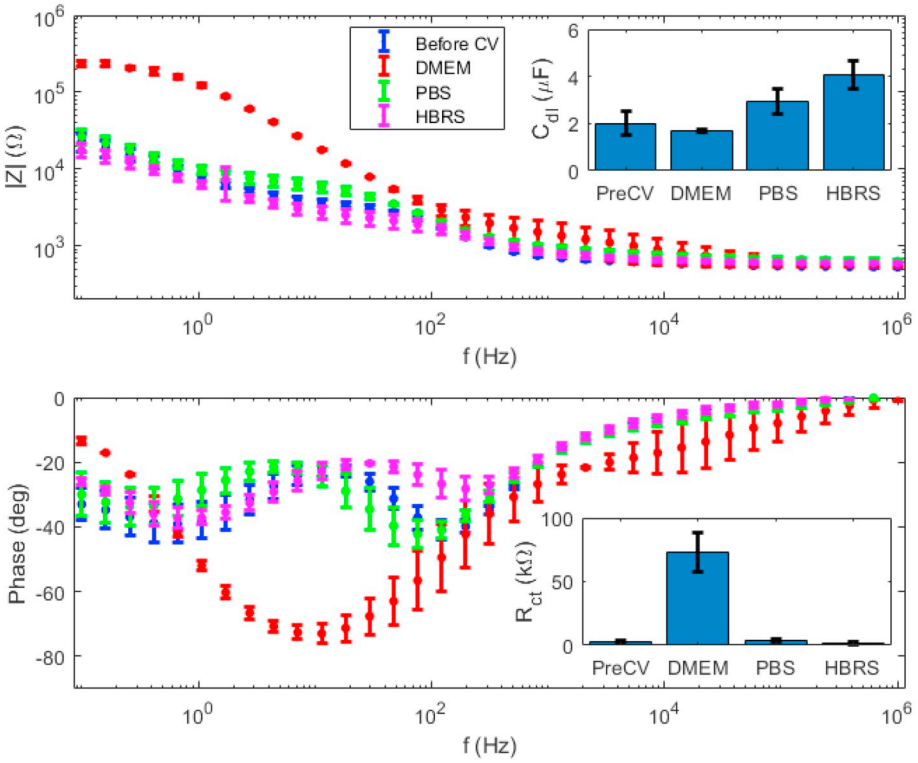

Fig. 4. Bode diagrams of the EIS data before and after the CVs in PBS, HBRS, and DMEM. The double layer capacitance and the charge transfer resistance values obtained by data fitting are reported in the impedance module and in the phase insets, respectively.

DMEM shows completely different EIS spectra, with a huge charge transfer contribution at the lowest frequencies and an unusual constant phase response between 1 kHz and 10 kHz, thus it was modeled by the EEC of Scheme 1b. Fig. 4 insets compares the results of the EIS data fits. In particular, we show the values obtained for the constant phase element representing the double layer capacitance, and for the charge transfer resistance. The C_{dl} values are obtained from the CPE definition:

$$Z_{CPE} = \frac{1}{j\,\omega\,C_{dl}{}^{n}} \quad with\ 0 \le n \le 1 \tag{2}$$

CV and EIS data suggest that a dielectric layer is adsorbed on the electrodes during CVs in DMEM. Indeed, this increases the charge transfer resistance during the EIS measurement in ferro/ferricyanide and creates a small capacitive contribution at high frequencies. Moreover, the drift of the CV current at 800 mV in DMEM indicates that the adsorption of the layer is time dependent, with a thicker layer after each cycle.

Since it is not clear if the electrode modification by DMEM prevents NADH detection on the DScs, we performed a NADH calibration in all the mediums/buffers, comparing the results. We tested NADH detection repeating the CVs on the same sensors, from the lowest to the highest concentration. To discriminate the currents related to NADH oxidation from the possible drift of the sensors response in the mediums/buffers, we repeated the same measurement setup without NADH, in a differential configuration. The calibration current values (i_{cal}) obtained with this configuration, were calculated as the difference between the peak current values of the CVs with ($i_p{}^{NADH}$) and without ($i_p{}^{no\ NADH}$) NADH for each medium/buffer, as described in the following:

$$i_{cal,i} = i_p^{NADH,i} - i_p^{no\ NADH,i}\ with\ i = 1,\ \ldots, number\ of\ NADH\ concentrations \tag{3}$$

The average calibration current values obtained by this analysis are depicted in Fig. 5 with the respective standard deviations.

To further validate our protocol, we also measured 3 NADH dilutions with one-shot measurements (reported as circles in the figure). The correspondence between these peak currents values with those obtained by Equ. 3 prove the absence of any interference from the respective medium/buffer and the validity of our method for the subtraction of the sensors drift. Moreover, this is a further step towards the use of the sensors also for continuous monitoring purposes, and not only for one-shot tests.

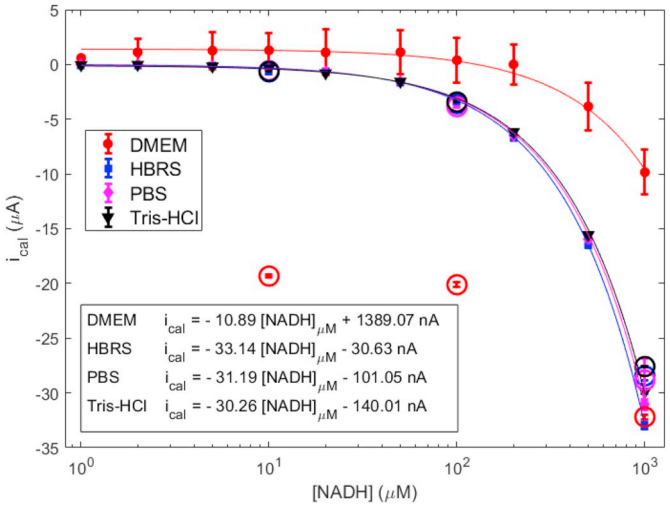

Fig. 5. Calibration current average values as a function of the NADH concentrations in the mediums/buffers as defined by Equ. 3. The lines represent the linear fits described in the textbox (curved by the semilogarithmic scale of the plot). The circles represent the peak currents obtained by the one-shot measurements.

The calibration currents obtained by the differential measurements have identical values for PBS, HBRS and Tris-HCl. Although in HBRS there were high voltage interferences, these did not affect the NADH detection, taking place at lower voltages.

DMEM shows a completely different behavior with current values dominated by interference, which cause a lower sensitivity to NADH in the differential configuration. Moreover, this is underlined also by the huge difference between the repeated and one-shot measurements.

The calibration currents recorded in differential configuration were fitted with linear models, defining a limit of detection of 10 µM and a linear response region between the LOD and at least 1 mM NADH for HBRS, PBS, and Tris-HCl. The sensitivity of the NADH quantification by the module of the CVs peak current was maximized in the HBRS cell medium with a slope of 33.14 nA/µM and the lowest intercept value. Therefore, all the following characterizations for the lactic acid catalysis have been performed in HBRS.

3.3. Lactic acid catalysis study

We studied the kinetics of the LDH-based LA catalysis in presence of 500 µM NAD^+ and of various LA dilutions in HBRS by UV–Vis absorbance measurements at 340 nm. We used this NAD concentration because we verified that higher concentrations show interferences of the 260 nm peak to the 340 nm one.

Fig. 6 shows the 340 nm absorbance values recorded over a period of 300 s during the lactate catalysis, i.e., the NADH formation, with three LDH enzyme concentrations, expressed in standard units (U) per milliliter. The bottom right plot shows the NADH formation rate (V), calculated as the slope the linear part of the curve–s in the previous plots, with respect to the tested LA concentration.

The LDH concentration influences both the kinetics stabilization time and the final values. With LDH concentration of 100 U/ml we found that all the kinetics stabilized in less than two minutes. The NADH formation rate values depicted in the bottom right plot of Fig. 6 were fitted by the Michaelis-Menten kinetics equation:

$$V = \frac{V_{max}\,[LA]}{K_M + [LA]} \tag{4}$$

The fit results are close to the experimental points (R^2 = 0.990) and the K_M and V_{max} values, i.e., the LA concentration at which the catalysis speed is half the maximum one, and the maximum catalysis speed, resulted 202.5 µM and 14.44 µM/min for the 100 U/ml protocol, respectively.

Interestingly, the obtained results could seem in disaccord with the adopted LDH concentrations, since the enzyme unit (U) is theoretically defined as the amount of the enzyme that catalyzes the conversion of 1 micro-mole of NAD^+ to NADH per minute at a temperature of 25 °C and a pH value and substrate concentration that yield the maximal substrate conversion rate. However, the enzyme units of the studied enzyme isoform (rabbit muscle) are referred to the reverse reaction, which catalyzes the conversion of Pyruvic acid (PA) to LA, that is much cheaper and easier to be found in commerce.

With the defined catalysis protocol, i.e., the 100 U/ml one, we performed the calibration of the electrochemical sensors in two steps. First, we performed the LA catalysis and we monitored it at 340 nm by the UV–Vis measurements (Fig. 7, bottom inset). Then, we drop-casted on the DSCs 100 µl of the solution obtained at the end of the kinetics, testing it by CV (Fig. 7, top inset). The module of the CV peak currents showed an excellent correlation with the UV–Vis determined NADH concentrations (R^2 = 0.999), with a slope coherent to the previously obtained one, depicted in Fig. 5. The obtained CV peak currents values were then used to define the sensor calibration curve to LA (Fig. 8). The performance factors of the sensor are reported in Table Error! Reference source not found.

The same LA samples tested with the LDH protocol were tested also by the LDH-GPT protocol (reported in Table A.2) to compare the two

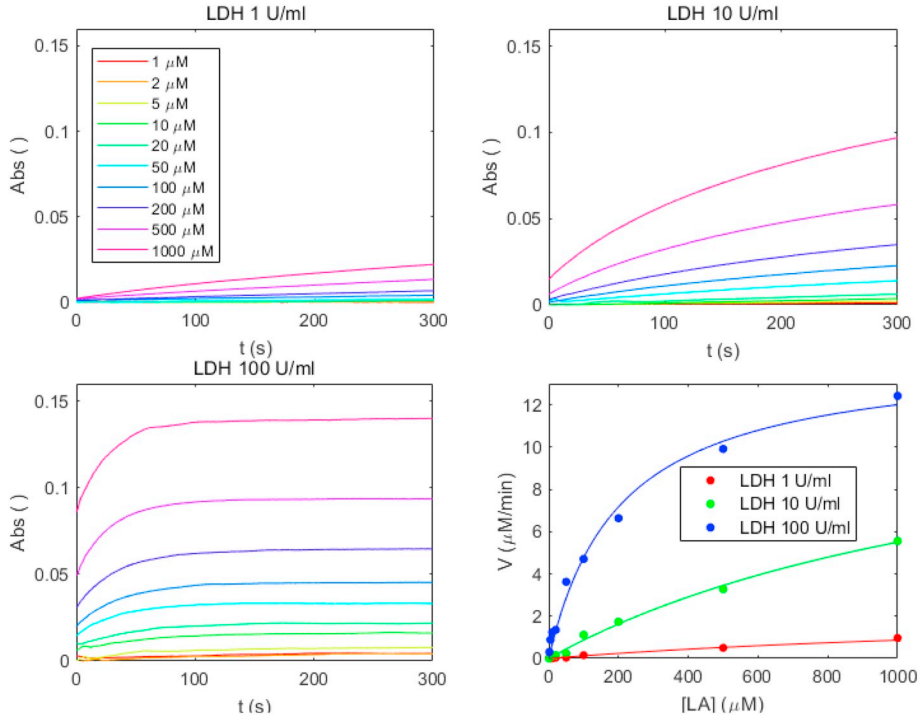

Fig. 6. UV–Visible 340 nm kinetics of the catalysis of 10 LA dilutions in HBRS with 500 µM NAD^+ and 3 LDH enzyme concentrations. The bottom right plot represents the NADH formation rate (V) as a function of the LA concentration and the respective Michaelis-Menten kinetic fits.

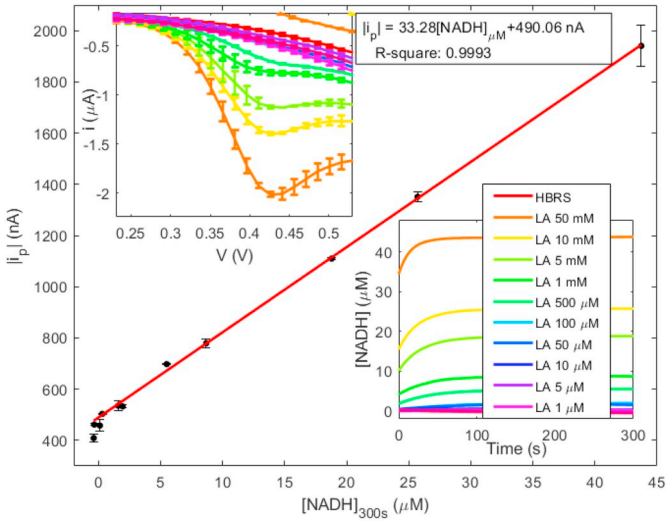

Fig. 7. Correlation curve and linear fit of the CV peak currents and the UV–Vis measured NADH concentrations. The bottom inset shows the UV–Vis kinetics at 340 nm of the NADH formation with the LDH protocol. The top inset shows a magnification of the NADH oxidation current peaks recorded during the CV measurements of the solutions at the end of the kinetics.

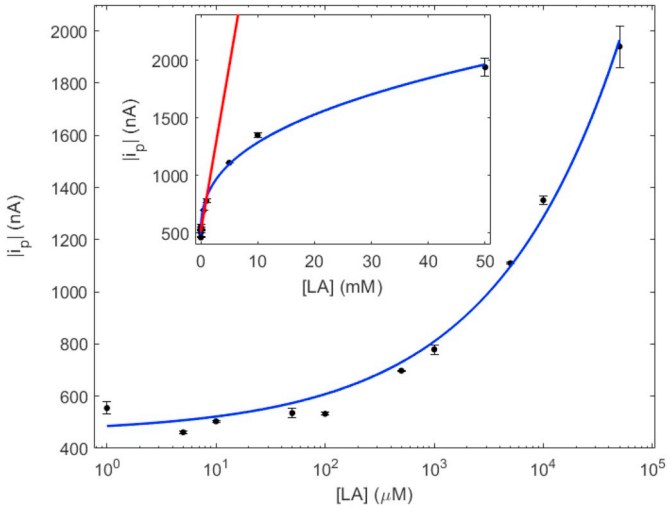

Fig. 8. Lactic acid calibration curve obtained by the CV peak current values in both logarithmic and linear scale. The points were fitted by a Langmuir law (blue) and a linear one (red). (For interpretation of the references to colour in this figure legend, the reader is referred to the web version of this article.)

methods. Before recording the UV–Vis 340 nm kinetics, we mixed the sample with all the reagents except the LDH enzyme. Then, we waited 3 min for stabilization. After that, the absorbance value is recorded (A_1) and the enzyme added to the solution. At the end of the 10 min' kinetics, the second and stable absorbance value is recorded (A_2). The formed NADH concentration is calculated by the following equation:

$$[NADH] = \frac{V}{\varepsilon\, d\, v}(A_2 - A_1) \tag{5}$$

where V is the total solution volume in the cuvette (in ml), ε is the extinction coefficient of NADH at 340 nm (6300 l·mol^{-1} cm^{-1}), d is the light path (1 cm), and v is the LA sample volume in the cuvette (in ml).

The same equation can be used also to calculate the NADH concentration produced by the LDH protocol but in this case, A_1 has to be set to zero since the used solutions do not absorb at 340 nm and the instrument is set to zero before the measurement.

Fig. 9 shows a comprehensive comparison between the LDH and LDH-GPT protocols in terms of the produced NADH by testing the same LA dilutions in HBRS. An effective way to compare the two protocols performances is the calculation of the catalysis efficiency in terms of the ratio between the produced NADH concentration and the lactate sample concentration. From this perspective, an ideal enzyme would convert all the lactate in the sample in NADH, obtaining a 100% [NADH]/[LA] efficiency, that would correspond to linear fits with unit slope. The inset

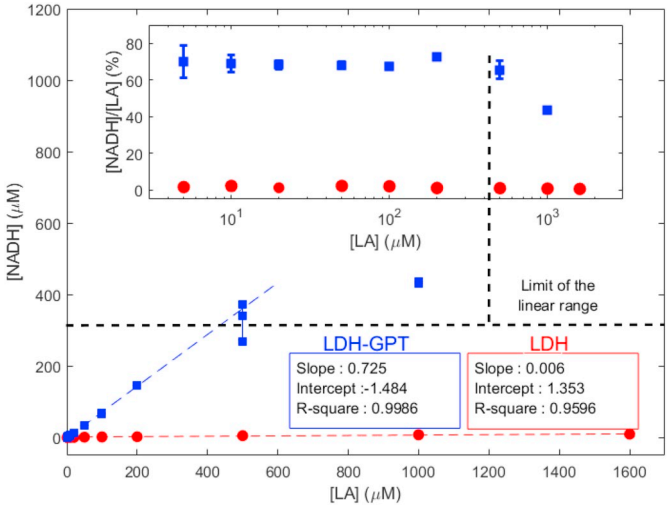

Fig. 9. Comparison of the NADH concentrations obtained by the LDH and the LDH-GPT protocols with respect to the LA concentrations, and the respective linear fits. The inset shows a comparison of the percentage catalysis efficiencies obtained with the two protocols.

of Fig. 9 (and the slopes of the linear fits in the textboxes) compares the ratios obtained by the tested LA samples with the two protocols.

It is clear that the LDH-GPT protocol dramatically boost the catalysis efficiency with respect to the standard LDH catalysis one, differing by 71.9%. The LA detection performance of the LDH-GPT protocol is hindered just at the highest concentrations by the spectrometer absorbance saturation.

The CV measurements of the LDH-GPT protocol are generally similar to those performed with the LDH protocol but the current peak moves to higher tensions. Therefore, in this case it has been necessary to consider the 600 mV current values instead of the peak current ones. The calibration study with the LDH-GPT protocol showed that the LA electrochemical detection has a sensitivity of 11.91 μA/mM, > 30 times the sensitivity obtained with the LDH protocol. Table 1 summarizes and compares the key performance factors of the two protocols.

An important feature of the LDH-GPT protocol is that the ratio between the sample volume and the total volume of the testing solution is drastically reduced from 1/10 to 1/22.4, thus the buffer/medium interference effects are reduced too. In fact, one of the case studies presented in the following has been performed in DMEM samples with negligible interference artifacts.

3.4. Case study 1: cell cultures analysis

As described in Section 2, the cells incubation was performed both in DMEM and in DMEM + 10% FBS for 72 h. Samples were taken every 24 h and the cell number was quantified right after sampling. The cell populations of each sample are reported in Table 2.

As expected, the cells showed a higher growth rate in presence of FBS rather than in pure DMEM.

Table 1
Performance factors of the LA detection protocols tested.

Performance factor	LDH protocol	Two-enzymes protocol
Sensitivity	0.38 μA/mM	11.91 μA/mM
LOD	5 μM	5 μM
Linear range	100–1000 μM	10–500 μM (modulable)
Response time	5 min* (UV–Vis) + 30 s (CV)	14 min* (UV–Vis) + 30 s (CV)
CV current peak tension	456 mV	600 mV

* The UV–Vis time can be considered as sample pretreatment time and decreased by multiplexing the samples (pretreating them in parallel).

Table 2
Cell populations (x 1000) in DMEM and in DMEM + 10% FBS after each sampling.

Time	24	48	72
DMEM	250	330	320
DMEM + 10% FBS	390	720	900

The collected samples were analyzed with the LDH-GPT protocol on the DSC devices and the obtained 600 mV current values were converted in LA concentration by the respective calibration curve. Fig. 10 shows the obtained LA concentrations for the cells and the medium samples in DMEM and in DMEM + 10% FBS.

The samples collected from the DMEM wells without cells had constant and negligible LA concentrations, while those collected from the cell cultures in DMEM showed a clear LA growth trend. For DMEM + 10% FBS, the LA concentration growth is even more evident, with values two times the previous ones. In this case, unlike DMEM, a constant bias is present in the wells without cells. However, the differential configuration allows to remove this effect of the interfering substances in FBS.

Therefore, the developed protocol proved to be effective for lactate detection in cell cultures within the standard medium DMEM and FBS, opening the way to real-time monitoring of cell cultures lactate concentration.

3.5. Case study 2: sweat analysis

LA detection in sweat during physical exercise was performed in two tests. During the first one, we verified that the LA concentration in sweat is not correlated with exercise intensity if the sweat rate is not taken into consideration, as previously verified by Buono et al. [48] and Sakharov et al. [49]. In fact, the increase of the LA concentration due to exercise intensity is masked by the dilution of the excreted LA in sweat, whose amount depends on temperature, humidity, and subject characteristics. Table 3 reports the LA concentrations measured during the first test.

The LA concentrations measured during the first test are high if compared to the typical blood values, which range between 0.01 and 0.11 mg/l. All the subjects, except subject 04, showed a decrease of the lactate values during the exercise, in accordance to the sampling artifact previously described. To compensate this artifact, we modified the sampling protocol and we introduced a method for the quantification of both the produced sweat amount and the sweat rate. As detailed in Section 3, we used an adsorbing lint placed under an impermeable membrane for each sample. The lint centrifugation allowed to measure the sweat amount by weighting, and thus the sweat rate dividing the amount by the sampling time (Equ. 1).

Fig. 11 shows the LA concentrations multiplied by the sweat sample masses as a function of both the exercise percentage intensity, and the blood LA concentration.

With this approach, the sweat LA concentration resulted well-correlated with both the exercise intensity and the blood LA levels. Even 2% exercise intensity variations resulted appreciable.

In conclusion, the LDH-GPT protocol, with appropriate sampling, proved to be valid for sweat lactate quantification with physical exercise monitoring applications. Moreover, our preliminary study offers an important guideline for possible wearable real-time biosensors implementation in this field.

4. Conclusions

In this work, we firstly analyzed the NADH detection by commercial SPCE. We found that these devices allow NADH oxidation at a potential as low as 456 mV, with a 10 μM LOD and a sensitivity of 33.14 nA/μM.

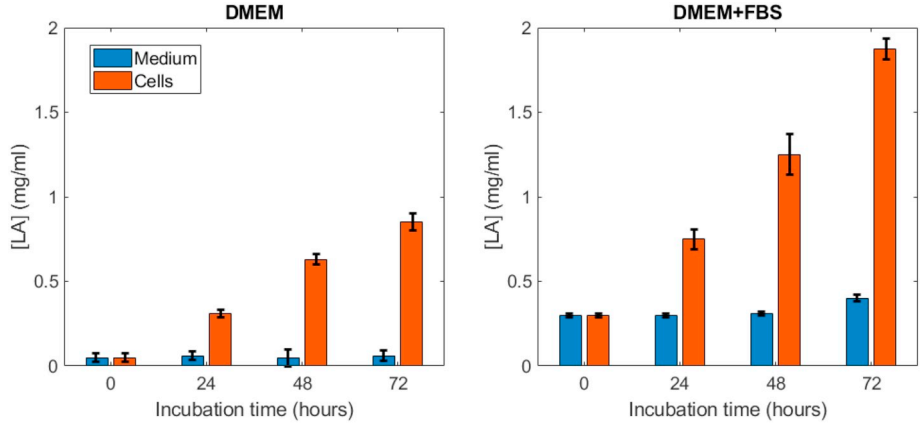

Fig. 10. LA concentrations obtained by the LDH-GPT protocol on DSC devices for the cells and medium samples in DMEM and in DMEM + 10% FBS.

Table 3
LA concentrations (in mg/l) measured by UV–Vis measurements with the LDH-GPT protocol in the first test samples from 4 healthy subjects every 10 min for 1 h of exercise at 45% PPO.

Subject/Sample	10 min	20 min	30 min	40 min	50 min	60 min
01	1.24	0.47	0.24	0.22	0.21	0.19
02	0.43	0.33	0.27	0.23	0.22	0.17
03	0.92	0.54	0.39	0.42	0.53	0.27
04	0.40	0.61	0.41	0.40	0.31	0.43

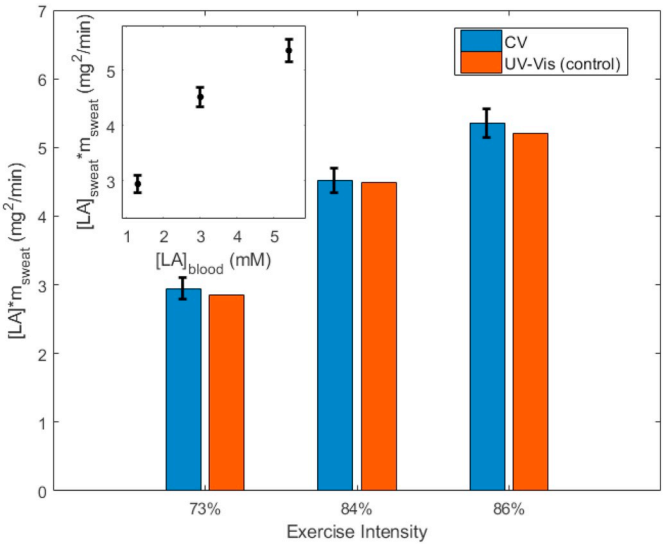

Fig. 11. LA concentrations multiplied by the sweat sample masses as a function of exercise intensity (a), and blood LA concentration (b). In (a), the values obtained by the UV–Vis and the CV measurements are compared.

Then, we characterized the interferences due to cell cultures mediums (DMEM and HBRS) and buffers (PBS and Tris-HCl) to NADH detection, both for repeated and one-shot measurements. We verified that DMEM physically alter the sensors, altering their response. However, we managed to find that HBRS allows to maintain cell cultures for several days, without affecting the NADH detection.

Then, we analyzed and compared two LA catalysis mechanisms by UV–Visible absorbance measurements and by Cyclic Voltammetries on the sensors. We found that a two-enzymes strategy based on LDH and GPT dramatically boost the catalysis efficiency from 0.6% to 72.5%. Moreover, this strategy allowed to minimize the DMEM interferences on the electrochemical NADH detection.

Finally, we proved the reliability and feasibility of the combination of this LDH-GPT catalysis mechanism with the electrochemical sensor for NADH detection as an easy and practical tool for LA quantification in two case studies. In the first one, we used the system to monitor the lactate production of a cell culture over 72 h of incubation. We observed a drastic increase of the lactate concentration over this period. In the second case study, we analyzed the correlation between physical exercise and the LA concentration in sweat, finding a valid sampling protocol and an interesting correlation of the sweat lactate with both the exercise intensity and the blood lactate levels.

In conclusion, this work presents a simple and affordable high efficiency method for lactate detection that can be used within cell cultures and physical exercise studies.

Patient consent

Consent to publish the case report was not obtained. This report does not contain any personal information that could lead to the identification of the patient.

Funding

This work has been partially supported by the regional project Myoscreen2 and the FSE project LactiSport, founded by Regione Veneto.

Authorship

All authors attest that they meet the current ICMJE criteria for Authorship.

Conflict of interest

The following authors have no financial disclosures: G. Rosati, G. Gherardi, D. Grigoletto, G. Marcolin, L. Cancellara, C. Mammucari, M. Scaramuzza, A. De Toni, C. Reggiani, R. Rizzuto, A. Paccagnella.

Table A.1
Comparison of the DMEM, HBRS and PBS compositions in mg/l.

Components(mg/l)	DMEM	HBRS	PBS
Amino acids			
Glycine	30		
L-Alanine	84		
L-Cystine 2HCl	63		
L-glutamine	580		
L-Histidine hydrochloride-H2O	42		

(*continued on next page*)

Table A.1 (*continued*)

Components(mg/l)	DMEM	HBRS	PBS
L-Isoleucine	105		
L-Leucine	105		
L-Lysine hydrochloride	146		
L-Methionine	30		
L-Phenylalanine	66		
L-Serine	42		
L-Threonine	95		
L-Tryptophan	16		
L-Tyrosine disodium salt dihydrate	72		
L-Valine	94		
Vitamins			
Choline chloride	4		
D-Calcium pantothenate	4		
Folic Acid	4		
Niacinamide	4		
Pyridoxine hydrochloride	4		
Riboflavin	0.4		
Thiamine hydrochloride	4		
i-Inositol	7.2		
Inorganic salts			
Calcium Chloride (CaCl2) (anhyd.)	264	294	100
Cupric Sulfate (CuSO4-5H2O)	0.1		
Ferric Nitrate (Fe(NO3)3"9H2O)			
Ferric Sulfate (FeSO4-7H2O)			
Magnesium Chloride (anhydrous)		204	
Magnesium Sulfate (MgSO4) (anhyd.)	200		47
Potassium Chloride (KCl)	400	370	200
Sodium Bicarbonate (NaHCO3)	3700		
Sodium Chloride (NaCl)	6400	9058	8000
Sodium Phosphate dibasic (Na2HPO4) anhydrous			
Sodium Phosphate monobasic (NaH2PO4-H2O)	141	276	1150
Zinc sulfate (ZnSO4-7H2O)			
Potassium Phosphate monobasic (KH2PO4)			200
Other components			
D-Glucose (Dextrose)	4500	1800	
Phenol Red	15		
Hepes		2384	

Table A.2
Megazyme L-lactate Assay kit protocol.

Solution	Blank	Sample
Distilled water (25 °C)	1.6 ml	1.5 ml
Sample	\	0.1 ml
Buffer	0.5 ml	0.5 ml
NAD/PVP	0.1 ml	0.1 ml
D-GPT	0.02 ml	0.02 ml
Mix by gentle inversion and read the absorbance after 3 min (A1)		
L-LDH	0.02 ml	0.02 ml
Mix by gentle inversion and read the absorbance after 10 min (A2)		

References

[1] K. Rathee, V. Dhull, R. Dhull, S. Singh, Biosensors based on electrochemical lactate detection: a comprehensive review, Biochemistry and Biophysics Reports 5 (2016) 35–54, https://doi.org/10.1016/j.bbrep.2015.11.010.

[2] T. Alizadeh, S. Nayeri, S. Mirzaee, A high performance potentiometric sensor for lactic acid determination based on molecularly imprinted polymer/MWCNTs/PVC nanocomposite film covered carbon rod electrode, Talanta 192 (2019) 103–111, https://doi.org/10.1016/j.talanta.2018.08.027 May 2018.

[3] G. Rosati, M. Scaramuzza, E. Pasqualotto, A. De Toni, C. Reggiani, A. Paccagnella, Modeling of SAM Impedance Onto Gold and Silver Thin-Film Mass-Produced Electrodes and their use for Optimization of Lactic Acid Detection, IEEE Transactions on NanoBioscience 15 (7) (2016) 756–764, https://doi.org/10.1109/TNB.2016.2616194.

[4] M. Scaramuzza, A. Ferrario, E. Pasqualotto, G. Rosati, A. De Toni, M. Quarta, A. Paccagnella, C. Reggiani, Low-cost Enzyme-based Biosensor for Lactic Acid Amperometric Detection - Electrical Modeling and Validation for Clinical and Food Processing Applications, Proceedings of the International Conference on Biomedical Electronics and Devices, 2012, pp. 380–383 (ISBN: 978-989-8425-91-1), https://doi.org/10.5220/0003867603800383.

[5] J. De Ruyck, M. Famerée, J. Wouters, E.a. Perpète, J. Preat, D. Jacquemin, Towards the understanding of the absorption spectra of NAD(P)H/NAD(P)+ as a common indicator of dehydrogenase enzymatic activity, Chem. Phys. Lett. 450 (1–3) (2007) 119–122, https://doi.org/10.1016/j.cplett.2007.10.092.

[6] M. Piano, S. Serban, R. Pittson, G. a Drago, J.P. Hart, Amperometric lactate biosensor for flow injection analysis based on a screen-printed carbon electrode containing Meldola's Blue-Reinecke salt, coated with lactate dehydrogenase and NAD+, Talanta 82 (1) (2010) 34–37, https://doi.org/10.1016/j.talanta.2010.03.051.

[7] M.M. Rahman, M.J. a Shiddiky, M.A. Rahman, Y.-B. Shim, A lactate biosensor based on lactate dehydrogenase/nictotinamide adenine dinucleotide (oxidized form) immobilized on a conducting polymer/multiwall carbon nanotube composite film, Anal. Biochem. 384 (1) (2009) 159–165, https://doi.org/10.1016/j.ab.2008.09.030.

[8] H.C. Yoon, H. Kim, Electrochemical characteristics of a carbon-based thick-film L-lactate biosensor using L-lactate dehydrogenase, Anal. Chim. Acta 336 (1996) 57–65.

[9] F. Ricci, A. Amine, D. Moscone, G. Palleschi, A probe for NADH and H2O2 amperometric detection at low applied potential for oxidase and dehydrogenase based biosensor applications, Biosens. Bioelectron. 22 (6) (2007) 854–862, https://doi.org/10.1016/j.bios.2006.03.004.

[10] S. Serban, N. El Murr, Redox-flexible NADH oxidase biosensor: a platform for various dehydrogenase bioassays and biosensors, Electrochim. Acta 51 (24) (2006) 5143–5149, https://doi.org/10.1016/j.electacta.2006.03.052.

[11] A. Radoi, D. Compagnone, Recent advances in NADH electrochemical sensing design, Bioelectrochemistry (Amsterdam, Netherlands) 76 (1–2) (2009) 126–134, https://doi.org/10.1016/j.bioelechem.2009.06.008.

[12] Z.-H. Dai, F.-X. Liu, G.-F. Lu, J.-C. Bao, Electrocatalytic detection of NADH and ethanol at glassy carbon electrode modified with electropolymerized films from methylene green, J. Solid State Electrochem. 12 (2) (2007) 175–180, https://doi.org/10.1007/s10008-007-0378-1.

[13] D.G. Dilgin, D. Gligor, H.I. Gökçel, Z. Dursun, Y. Dilgin, Photoelectrocatalytic oxidation of NADH in a flow injection analysis system using a poly-hematoxylin modified glassy carbon electrode, Biosens. Bioelectron. 26 (2) (2010) 411–417, https://doi.org/10.1016/j.bios.2010.07.120.

[14] L. Gorton, Electrocatalytic oxidation of NAD (P) H at mediator-modified electrodes, Rev. Mol. Biotechnol. 82 (2002) 371–392.

[15] V. Lates, D. Gligor, L.M. Muresan, I.C. Popescu, Comparative investigation of NADH electrooxidation at graphite electrodes modified with two new phenothiazine derivatives, J. Electroanal. Chem. 661 (1) (2011) 192–197, https://doi.org/10.1016/j.jelechem.2011.07.046.

[16] B. Prieto-Simón, E. Fàbregas, Comparative study of electron mediators used in the electrochemical oxidation of NADH, Biosens. Bioelectron. 19 (10) (2004) 1131–1138, https://doi.org/10.1016/j.bios.2003.10.010.

[17] B. Prieto-Simón, J. Macanás, M. Muñoz, E. Fàbregas, Evaluation of different mediator-modified screen-printed electrodes used in a flow system as amperometric sensors for NADH, Talanta 71 (5) (2007) 2102–2107, https://doi.org/10.1016/j.talanta.2006.09.022.

[18] G.P. Keeley, A.O. Neill, M. Holzinger, S. Cosnier, J.N. Coleman, G.S. Duesberg, DMF-exfoliated graphene for electrochemical NADH detection, Phys. Chem. Chem. Phys. 13 (2011) 7747–7750, https://doi.org/10.1039/c1cp20060g.

[19] M. Musameh, J. Wang, A. Merkoci, Y. Lin, Low-potential stable NADH detection at carbon-nanotube-modified glassy carbon electrodes, Electrochem. Commun. 4 (10) (2002) 743–746, https://doi.org/10.1016/S1388-2481(02)00451-4.

[20] K.S. Prasad, J.-C. Chen, C. Ay, J.-M. Zen, Mediatorless catalytic oxidation of NADH at a disposable electrochemical sensor, Sensors Actuators B Chem. 123 (2) (2007) 715–719, https://doi.org/10.1016/j.snb.2006.10.012.

[21] C.R. Raj, S. Behera, Mediatorless voltammetric oxidation of NADH and sensing of ethanol, Biosens. Bioelectron. 21 (6) (2005) 949–956, https://doi.org/10.1016/j.bios.2005.03.001.

[22] L. Zhang, Y. Li, L. Zhang, D.-W. Li, D. Karpuzov, Y.-T. Long, Electrocatalytic Oxidation of NADH on Graphene Oxide and Reduced Graphene Oxide Modified Screen-Printed Electrode, Int. J. Electrochem. Sci. 6 (2011) 819–829.

[23] A. Qureshi, W.P. Kang, J.L. Davidson, Y. Gurbuz, Review on carbon-derived, solid-state, micro and nano sensors for electrochemical sensing applications, Diam. Relat. Mater. 18 (12) (2009) 1401–1420, https://doi.org/10.1016/j.diamond.2009.09.008.

[24] N. Thiyagarajan, J.-L. Chang, K. Senthilkumar, J.-M. Zen, Disposable electrochemical sensors: a mini review, Electrochem. Commun. 38 (2014) 86–90, https://doi.org/10.1016/j.elecom.2013.11.016.

[25] C. You, Y. Xuewu, Y. Wang, S. Zhang, J. Kong, D. Zhao, B. Liu, Electrocatalytic

oxidation of NADH based on bicontinuous gyroidal mesoporous carbon with low overpotential, Electrochem. Commun. 11 (1) (2009) 227–230, https://doi.org/10.1016/j.elecom.2008.11.011.
[26] E. Katekawa, F. Maximiano, L.L. Rodrigues, M. Flávia Delbem, S.H. Serrano, Electrochemical oxidation of NADH at a bare glassy carbon electrode in different supporting electrolytes, Anal. Chim. Acta 385 (1–3) (1999) 345–352, https://doi.org/10.1016/S0003-2670(98)00694-1.
[27] G. Rosati, M. Scaramuzza, V. Rotilio, L. Monaco, E. Pasqualotto, F. Campolo, A. De Toni, C. Reggiani, F. Naro, A. Paccagnella, Culture Mediums and Buffer effect on Screen-printed Carbon Electrodes for Continuous Voltammetric monitoring of in vitro Cell Cultures Lactate Production, Procedia Technology 27 (2017) 246–247 ISSN 2212-0173 https://doi.org/10.1016/j.protcy.2017.04.105.
[28] G. Rosati, M. Scaramuzza, E. Pasqualotto, A. De Toni, A. Paccagnella, Optimization of Cyclic Voltammetric Curve Parameters to Measure Lactate Concentration in Urine Samples, in: B. Andò, F. Baldini, C. Di Natale, G. Marrazza, P. Siciliano (Eds.), Sensors. CNS 2016. Lecture Notes in Electrical Engineering, Springer, Cham, 2018, p. 431.
[29] J.H. Griffint, R.S. Criddle, Substrate-Inhibited Lactate Dehydrogenase. Reaction Mechanism and Essential Role, Biochemistry 9 (5) (1966) 1195–1205.
[30] Tsao, Y. S., Cardoso, A. G., Condon, R. G. G., Voloch, M., Lio, P., Lagos, J. C., … Liu, Z. (2005). Monitoring Chinese hamster ovary cell culture by the analysis of glucose and lactate metabolism. TL - 118. J. Biotechnol., 118 VN - (3), 316–327. https://doi.org/10.1016/j.jbiotec.2005.05.016
[31] N.R. Abu-Absi, B.M. Kenty, M.E. Cuellar, M.C. Borys, S. Sakhamuri, D.J. Strachan, … Z.J. Li, Real time monitoring of multiple parameters in mammalian cell culture bioreactors using an in-line Raman spectroscopy probe, Biotechnol. Bioeng. 108 (5) (2011) 1215–1221, https://doi.org/10.1002/bit.23023.
[32] S. Hisiger, M. Jolicoeur, Plant cell culture monitoring using an in situ multi-wavelength fluorescence probe, Biotechnol. Prog. 21 (2) (2005) 580–589, https://doi.org/10.1021/Bp049726f.
[33] F.J. Rawson, A.J. Downard, K.H. Baronian, Electrochemical detection of intracellular and cell membrane redox systems in Saccharomyces cerevisiae, Sci. Rep. 4 (2014) 1–9, https://doi.org/10.1038/srep05216.
[34] X.T. Zheng, H. Bin Yang, C.M. Li, Optical detection of single cell lactate release for cancer metabolic analysis, Anal. Chem. 82 (12) (2010) 5082–5087, https://doi.org/10.1021/ac100074n.
[35] J. Kruid, R. Fogel, J. Limson, Voltammetric investigation of complex growth media at a bare glassy carbon electrode: a case study of oxytetracycline, Electrochim. Acta 128 (2014) 41–47, https://doi.org/10.1016/j.electacta.2013.08.188.
[36] M.C. Garcia-Alonso, L. Saldana, C. Alonso, V. Barranco, M.A. Munoz-Morris, M.L. Escudero, In situ cell culture monitoring on a Ti-6Al-4V surface by electrochemical techniques, Acta Biomater. 5 (4) (2009) 1374–1384, https://doi.org/10.1016/j.actbio.2008.11.020.
[37] I.O.K. Owino, O.A. Sadik, Impedance Spectroscopy: a Powerful Tool for Rapid Biomolecular Screening and Cell Culture monitoring, Electroanalysis 17 (23) (2005) 2101–2113, https://doi.org/10.1002/elan.200503371.
[38] A.R.A. Rahman, Cell culture monitoring by impedance mapping using a multi-electrode scanning impedance spectroscopy system (CellMap), Physiol. Meas. 227 (2008) 227–239, https://doi.org/10.1088/0967-3334/29/6/S20.
[39] J. Wang, C. Wu, N. Hu, J. Zhou, L. Du, P. Wang, Microfabricated Electrochemical Cell-based Biosensors for Analysis of living Cells in Vitro, Bios 2 (2) (2012) 127–170, https://doi.org/10.3390/bios2020127.
[40] G. Rosati, J. Daprà, S. Cherré, N. Rozlosnik, Performance Improvement by Layout designs of Conductive Polymer Microelectrode based Impedimetric Biosensors, Electroanalysis 26 (2014) 1400–1408, https://doi.org/10.1002/elan.201400062.
[41] G. Rosati, L. Sappia, R. Madrid, N. Rozlòsnik, Iron(III)-Tosylate Doped PEDOT and PEG: a Nanoscale Conductivity Study of an Electrochemical System with Biosensing applications, International Journal of Medical, Health, Biomedical, Bioengineering and Pharmaceutical Engineering 131 (11) (2017) 597.
[42] M.L. Goodwin, J.E. Harris, A. Hernández, L.B. Gladden, Blood lactate measurements and analysis during exercise: a guide for clinicians, J. Diabetes Sci. Technol. 1 (4) (2007) 558–569, https://doi.org/10.1177/193229680700100414.
[43] S. Cairns, Lactic Acid and Exercise Performance, Sports Med. 36 (4) (2006) 279–291, https://doi.org/10.2165/00007256-200636040-00001.
[44] A.J. Bandodkar, D. Molinnus, O. Mirza, T. Guinovart, J.R. Windmiller, G. Valdés-Ramírez, J. Wang, Epidermal tattoo potentiometric sodium sensors with wireless signal transduction for continuous non-invasive sweat monitoring, Biosens. Bioelectron. 54 (2014) 603–609, https://doi.org/10.1016/j.bios.2013.11.039.
[45] D. Morris, S. Coyle, Y. Wu, K.T. Lau, G. Wallace, D. Diamond, Bio-sensing textile based patch with integrated optical detection system for sweat monitoring, Sensors Actuators B Chem. 139 (1) (2009) 231–236, https://doi.org/10.1016/j.snb.2009.02.032.
[46] S. Anastasova, B. Crewther, P. Bembnowicz, V. Curto, H.M. Ip, B. Rosa, G.Z. Yang, Corrigendum to “A wearable multisensing patch for continuous sweat monitoring” (Biosensors and Bioelectronics (2016) 93 (139–145) (S0956566316309198) (10.1016/j.bios.2016.09.038)), Biosens. Bioelectron. 94 (September 2016) (2017) 730, https://doi.org/10.1016/j.bios.2017.03.018.
[47] G. Borg, Psychophysical scaling with applications in physical work and the perception of exertion, Scand. J. Work Environ. Health 16 (Suppl. 1) (1990) 55–58, https://doi.org/10.5271/sjweh.1815.
[48] M.J. Buono, N.V.L. Lee, P.W. Miller, The relationship between exercise intensity and the sweat lactate excretion rate, J. Physiol. Sci. 60 (2) (2010) 103–107, https://doi.org/10.1007/s12576-009-0073-3.
[49] D.A. Sakharov, M.U. Shkurnikov, M.Y. Vagin, E.I. Yashina, A.A. Karyakin, A.G. Tonevitsky, Relationship between lactate concentrations in active muscle sweat and whole blood, Bull. Exp. Biol. Med. 150 (1) (2010) 83–85, https://doi.org/10.1007/s10517-010-1075-0.